Stromal Cell Identity Modulates Vascular Morphogenesis in a Microvasculature-on-a-Chip Platform

Journal:	*Lab on a Chip*
Manuscript ID	LC-ART-10-2020-001092.R1
Article Type:	Paper
Date Submitted by the Author:	15-Jan-2021
Complete List of Authors:	Margolis, Emily; University of Michigan, Biomedical Engineering Cleveland, David; University of Michigan, Internal Medicine Kong, Yen; University of Michigan, Biomedical Engineering Beamish, Jeffrey; University of Michigan, Internal Medicine Wang, William; University of Michigan Department of Biomedical Engineering, Biomedical Engineering Baker, Brendon; University of Michigan, Biomedical Engineering Putnam, Andrew; University of Michigan, Biomedical Engineering

January 15th, 2021

Stromal Cell Identity Modulates Vascular Morphogenesis in a Microvasculature-on-a-Chip Platform

Emily A. Margolis[1], David S. Cleveland[2], Yen P. Kong[1], Jeffrey A. Beamish[2], William Y. Wang, Brendon M. Baker, and Andrew J. Putnam[1]*

[1]Department of Biomedical Engineering, University of Michigan
[2]Department of Internal Medicine, University of Michigan

*Corresponding Author:
Andrew Putnam
University of Michigan
2204 Lurie Biomedical Eng. Bldg.
1101 Beal Ave.
Ann Arbor, MI 48109
Phone: (734) 615-1398
Email: putnam@umich.edu

ABSTRACT

Supportive stromal cells of mesenchymal origins regulate vascular morphogenesis in developmental, pathological, and regenerative contexts, contributing to vessel formation, maturation, and long-term stability, in part via the secretion of bioactive molecules. In this work, we adapted a microfluidic lab-on-a-chip system that enables the formation and perfusion of microvascular capillary beds with connections to arteriole-scale endothelialized channels to explore how stromal cell (SC) identity influences endothelial cell (EC) morphogenesis. We compared and contrasted lung fibroblasts (LFs), dermal fibroblasts (DFs), and bone marrow-derived mesenchymal stem cells (MSCs) for their abilities to support endothelial morphogenesis and subsequent perfusion of microvascular networks formed in fibrin hydrogels within the microfluidic device. We demonstrated that while all 3 SC types supported EC morphogenesis, LFs in particular resulted in microvascular morphologies with the highest total network length, vessel diameter, and vessel interconnectivity across a range of SC-EC ratio and density conditions. Not only did LFs support robust vascular morphology, but also, they were the only SC type to support functional perfusion of the resultant capillary beds. Lastly, we identified heightened traction stress produced by LFs as a possible mechanism by which LFs enhance endothelial morphogenesis in 3D compared to other SC types examined. This study provides a unique comparison of three different SC types and their role in supporting the formation of microvasculature that could provide insights for the choice of cells for vascular cell-based therapies and the regulation of tissue-specific vasculature.

INTRODUCTION

Capillaries are necessary to transport blood, oxygen, and other nutrients throughout the body. Vascularization of engineered tissues is required to avoid tissue death and allow convective transport of nutrients in metabolically active tissues that are too thick to be sustained via diffusion alone.[1] An important objective in biomedical engineering is to create functional (perfusable) capillary networks that can rapidly inosculate with host blood vessels upon transplantation to regenerate large tissue volumes. The ability to create functional and stable blood vessels remains a significant hurdle in the clinical implantation of nearly all engineered tissues;[2] without microvasculature, tissues greater than 200 μm in thickness cannot remain viable.[3] Existing methods to form functional vasculature include creating prepatterned vessel structures seeded with endothelial cells[4,5] or harnessing existing vasculature's ability to undergo angiogenesis to create new vessels.[6] While these methods can create vasculature in as short as 3 days, the vessels often lack supportive mural cells required to maintain long-term function and stability *in vivo.*[7,8]

Another approach to achieving neovascularization involves vascular self-assembly, which occurs when endothelial cells (ECs) and stromal cells (SCs) are co-cultured in three-dimensional hydrogels and undergo a process akin to developmental vasculogenesis. Our group has developed several assays to investigate neovascularization in the presence of multiple SC types including sprouting vascular bead assays,[9,10,11] vasculogenesis in bulk hydrogels,[12–14] and vasculogenesis in modular microtissues.[15] However, these methods lack the ability to study perfusion of microvessels in a physiologic manner *in vitro*. In this study, we examined the ability of various SCs to aid the formation of functional microvasculature when co-cultured with ECs in a perfusable microfluidic system. While the creation of microvasculature using co-culture systems within microfluidic platforms has been previously explored,[16–18] comparisons across systems have been limited by differences in microfluidic geometries, endothelial cell lineages, types of anastomoses (i.e., to openings in PDMS channels or to

endothelialized vessels), and culture duration. In this study, we directly compared the abilities of different SCs to modulate network formation and function within a single physiologically-relevant model system. Notable key features in our comparison were the use of a consistent EC source to isolate the effect of SCs and the use of endothelialized channels within the hydrogel to simulate biologically relevant inosculation of microvessels to arteriole-scale vessel structures rather than PDMS channels (endothelial cell lined or not) in a chip. In the present study, we successfully developed a widespread capillary bed within a microfluidic hydrogel and deciphered the roles of each SC type in modulating vessel formation and perfusion over time. The three SC types chosen for this study (LFs, DFs, and MSCs) are known to support vessel formation in a rage of 3D culture systems. LFs have been shown to robustly support vascular morphogenesis of various EC types.[9] DFs and MSCs potentially represent more clinically relevant cell sources capable of supporting vascular morphogenesis,[12,19] accessible via skin biopsy and bone marrow isolation, respectively. MSCs in particular secrete pro-angiogenic factors[20–22] and are capable of taking on a pericyte phenotype[16,23] important for vessel maturation and stability over extended culture periods. We measured multiple properties of the resultant microvascular networks pertaining to both formation and function to capture differences in the support provided by each SC type, finding that the degree of vascular formation and function were dependent on the SC type used to support microvascular networks. This study highlights the need for more comparative studies elucidating key differences in commonly used cell types and possible mechanisms underlying vascular formation and function.

MATERIALS AND METHODS

Cell culture

Human umbilical vein endothelial cells (ECs) were isolated from fresh umbilical cords (obtained via an IRB-exempt protocol from the University of Michigan Mott's Children's Hospital), cultured

in fully supplemented endothelial growth medium-2 (EGM-2; Lonza, Walkersville, MD), and used until passage 7. Bone marrow derived mesenchymal stem cells (MSCs; RoosterBio, Frederick, MD) were cultured in Rooster Nourish (RoosterBio) and used until passage 7. Normal human dermal fibroblasts (DFs; Lonza) and normal human lung fibroblasts (LFs; Lonza) were cultured in high glucose Dulbecco's modified eagle medium (DMEM; Gibco, Waltham, MA) supplemented with 10% fetal bovine serum (FBS; Gibco) and used until passage 15. All cells were cultured at 37 °C and 5% CO_2 with medium exchanges every other day.

Vasculogenesis assay within microfluidic chip platform

A vasculogenesis assay widely used in our lab[12,13] was modified for use within a microfluidic chip system (Fig. 1).[24] SCs and ECs suspended in serum free EGM-2 were combined at 2:1 (2M/mL SCs with 1M/mL ECs or 1M/mL SCs with 500K/mL ECs) or 1:1 (1M/mL of each cell type or 500K/mL of each cell type) ratios (Table 1),[17,18,22,25] encapsulated in fibrin precursor solutions, and injected into insertion ports within the chip to polymerize around two 290 μm diameter needles (Fig. 1a, b). Precursor solutions contained 2.5 mg/mL (clottable protein) filtered bovine fibrinogen (Sigma, St. Louis, MO), 1 U/mL bovine thrombin (Sigma), and 10% FBS. Following gelation and swelling, needles were removed, needle tracks were sealed with vacuum grease (Dow Corning, Midland, MI), and empty channels were seeded with additional ECs suspended at 2.5 M/mL. Chips were statically cultured in fully supplemented EGM-2 exchanged daily (50 μL reservoir, 200 μL per sample) and cultured for one or two weeks. To confirm vascular formation using the specific combination of ECs and SCs within each device, cell-containing bulk fibrin hydrogels were created as described above, in 48-well culture plates, and cultured in EGM-2 for 7 days, with medium exchanges on days 1, 3, and 5. Chips were discarded if vascular formation was not observed in control gels.

Channel patency and network perfusion

On the final day of culture, fluorescein dextran (10 kDa, 25 μg/mL) was inserted into media reservoirs at a hydrostatic pressure difference of ~0.1 cmH$_2$O and imaged in real time. If dextran flowed through the channels, the channels were considered patent and if dextran flowed through vessel network, the network was considered perfused.

Immunofluorescence staining and imaging

Chips were fixed on the last day of culture on a rocker plate for 1 hour in 4% paraformaldehyde (Sigma) and washed with phosphate buffered saline (PBS; Gibco) for at least 12 hours. Bulk gels were fixed on day 7 for 15 minutes in aqueous buffered zinc formalin fixative (Z-fix; Anatech, Battle Creek, MI). Following fixation and washing, control gels and chips were permeabilized for 1 hour in 0.1% Triton-X 100 (Fisher Scientific, Waltham, MA) in PBS and blocked for 4 hours in blocking solution (2% bovine serum albumin (BSA; Sigma) dissolved in tris buffered saline-Tween20 (TBS-T; Fisher Scientific). Samples were stained overnight with rhodamine-conjugated Ulex europaeus Agglutinin I (UEA; Vector Laboratories, Burlingame, CA) at 1:200 dilution and 4', 6-diamidino-2-phenylindol (DAPI; 1µg/mL, Sigma) to label ECs and all cell nuclei, respectively. Staining dilutions were made in blocking solution. Following staining, samples were washed with TBS-T for at least 12 hours before imaging. TBS-T was exchanged after washing and before imaging. For all staining processes, chips were maintained on a rocker plate and control gels were maintained in static conditions.

Selected samples were further stained for alpha smooth muscle actin (αSMA) to identify SCs within the gels. Samples were incubated overnight at 4ºC with a primary antibody for αSMA (Sigma, A2547, mouse IgG$_{2a}$ isotype, 1:200 dilution) and washed with TBS-T overnight at 4ºC. Samples were then incubated overnight at 4ºC with an Alexa Fluor 488 conjugated secondary antibody (Invitrogen, A11001, goat-*anti*-mouse IgG$_{H+L}$, 1:200 dilution) and washed with TBS-T overnight at 4ºC. Antibody dilutions were made in blocking solution.

Images were acquired with an Olympus IX81 inverted fluorescent microscope equipped with a confocal Disc Spinning Unit (DSU; Olympus America, Center Valley, PA) and Metamorph Software (Molecular Devices, Sunnyvale, CA). Control gels were imaged to confirm the presence of vasculature, but not further quantified. Confocal z-stacks (4 slices/stack) of chips were obtained and compressed into maximum intensity projections preceding analysis. Quantification of total network length and network interconnectedness were performed on 225 μm stacks (75 μm/slice) obtained at 4x magnification. Quantification of vessel diameter and qualitative analysis of αSMA expression were performed on 30 μm stacks (10 μm/slice) obtained at 10x magnification. Images acquired at 4x spanned the region between the two parent channels and images acquired at 10x were in close proximity to the parent channels not the boundaries of the chip. Total network length per volume, number of connected vessel sets per volume, and vessel diameter were quantified using the Angiogenesis Tube Formation module in Metamorph (Fig. 1c). This program creates a binary mask of the fluorescent images based on user inputted values for threshold above background and minimum/maximum vessel size. Any region of the white mask that is within the user inputted size range is considered a vessel and is added to the total network length value; regions of the mask above the size range are considered nodes and not counted towards the network length value. Network interconnectedness is measured via the number of connected vessel sets, in which the program counts the number of separate, non-connected masked regions and determines the network length of each independent set. Vessel diameter is an average value for the image calculated by dividing total network area by total network length. Multiple images per sample were quantified and averaged to obtain a single value per sample for each metric. Cell counts were performed on 4x DAPI images. Images were binarized and nuclei were counted using a custom ImageJ script. The change in cell number was calculated as a percentage of the theoretical initial cell density.

Traction force microscopy

Traction force microscopy was performed on all three SC types, using previously described methods,[26–28] to gain an understanding of differences in the magnitude of tractional vectors produced by each SC type. Square cover glass (22 mm; VWR, Radnor, PA) was etched with piranha solution (1-part H_2O_2 (Fisher Scientific) with 3-parts sulfuric acid (Fisher Scientific)) and functionalized with 1% glutaraldehyde (Sigma). Two kPa polyacrylamide (PA) gels with 0.2 μm fluorescent beads (Invitrogen, Carlsbad, CA) were formed on top of the glass slides, followed by conjugation of 50 μg/mL type-I collagen (Advanced Biomatrix, San Diego, CA) via sulfo-sanpah (Proteochem, Hurricane, UT). Fluorescent beads in the PA gel served as displacement markers during imaging. Cells were seeded onto the gels at 1000 cells/mm^2. Individual cells and bead planes were imaged one day post-seeding both before and after cell lysis to measure bead displacements. Displacement vectors and traction were computed via the particle image velocimetry (PIV) and fourier transform traction cytometry (FTTC) plugins in ImageJ, respectively. Traction data were analyzed via a custom MATLAB (Mathworks, Natick, MA) script. Experimental number included 12-16 cells per slide and two slides per cell type, which were pooled together for statistical analysis.

Statistics

Prism 8 (GraphPad, San Diego, CA) was used to analyze data for statistical significance. All data are represented as mean $\pm$ standard deviation. Microfluidic chip data were analyzed with statistical tests performed on n = 3 independent replicates. For the independent replicates in each condition, data from 3-4 technical replicates were averaged together resulting in a single data point per independent replicate. Data were analyzed using a one-way ANOVA with Sidak's multiple comparisons post-hoc test for pre-specified comparisons. For TFM data, each cell was

considered an independent sample (n = 28-30 cells per condition across 2 different substrates) and the data were analyzed with a Kruskal-Wallis test with Dunn's multiple comparisons post-hoc test. $p < 0.05$ was considered statistically significant.

RESULTS

All three stromal cell types facilitate the formation of microvascular networks

We examined capillary network formation via a self-assembly process similar to developmental vasculogenesis within a microfluidic chip platform to enable studies of perfusion. We examined four different co-culture conditions (Table 1) that varied in cell density and SC-EC ratio in order to determine if these parameters in addition to SC identity influenced vascular morphogenesis. Past studies have examined differing densities and ratios further complicating cross-comparison between distinct studies. Therefore, we sought to enable these comparisons within a single multiplexed microfluidic chip system which facilitated the assessment of a broad range of conditions. LFs, DFs, and MSCs supported the formation of microvascular networks by day 7 (Fig. 2a, top & Fig. 2b, left) and by day 14 (Fig. 2a, bottom & Fig. 2b, right) across all conditions. Control samples containing only ECs were fabricated at two different cell densities: 1 M/mL and 500 K/mL. These controls showed that ECs fail to form stable networks in the absence of SCs by day 7 (Fig. S1).

To understand the quantity of vasculature formed we assessed the total length of microvascular networks formed in each condition. On day 7, networks formed with support from LFs and DFs exhibited significantly longer total network length (TNL) than networks formed with support from MSCs in all four conditions (Fig. 2b, left). LF-supported networks were significantly longer than DF-supported networks only at the highest (condition 1) and lowest (condition 4) initial cell densities tested (Fig. 2b, left). At intermediate cell densities (conditions 2 and 3), DFs were capable of supporting network formation to the same extent as LFs. By day 14, LF-supported networks exhibited greater TNL compared to DF-supported networks across

conditions 1-3, while DF-supported networks exhibited greater TNL compared to MSC-supported networks across conditions 2-4 (Fig. 2b, right). At the highest initial cell densities examined (condition 1), MSCs were capable of supporting network formation to the same extent as DFs; at the lowest initial cell densities tested (condition 4), LFs and DFs supported vascular morphogenesis to similar extents, with both significantly greater than MSCs. LFs consistently supported greater TNL than MSCs, regardless of condition. These studies indicate that fibroblasts aid more extensive vascular formation than MSCs.

After examining changes in TNL between the three SC types we aimed to determine if TNL increased over time for each SC type. Examining each SC type separately we compared each condition across time points (i.e., LFs condition 1 day 7 vs. LFs condition 1 day 14). MSC- and DF-supported networks did not display significant differences in TNL between day 7 and day 14 for networks of the same condition (Fig. 2c, middle and right). Conversely, LF-supported networks did display differences in one condition only, condition 3, which showed a significant increase in TNL by day 14 compared to day 7 (Fig. 2c left). We also sought to determine if TNL was maintained regardless of initial cell density, therefore, we examined differences on a single day for a single SC type across conditions (i.e., DFs condition 1 day 7 vs. DFs condition 3 day 7). LF-supported networks showed significant differences on day 14 between conditions 1 and 4 and between conditions 3 and 4, while DF- and MSC- supported networks displayed no significant differences between conditions at either timepoint. While not statistically significant, MSC-supported networks displayed a downward trend in network length as the initial cell density decreased. Taken together, these data suggest that all three SC types supported the formation of vasculature that was maintained over extended periods of culture without significant loss of network length due to vessel pruning or other network modifications.

We also quantified the effects of stromal cell identity on the diameter of the microvessels at day 14. LFs facilitated the formation of vessels with larger diameters compared to those formed in the presence of both DFs and MSCs (Fig. 2d, e). DF- and MSC-supported vessels

exhibited similar diameters that were not significantly different from each other in three of the four conditions (Fig. 2d). While LF-supported vessels were consistently larger than DF- and MSC-supported vessels, there were also differences in diameter between LF-supported vessels of different conditions (conditions 1 vs. 4 and conditions 3 vs. 4). The differences in diameter were between the same conditions that displayed differences in TNL. These data show that engineered capillaries formed with each of the three SC types had diameters on the order of capillary vessels *in vivo*, typically less than 50 μm.[29]

Stem cells are capable of supporting changes in network interconnectedness over time

With the exception of one condition (LFs, condition 3), networks formed by the same SC type did not exhibit significant differences in TNL between day 7 and day 14 (Fig. 2b, c); therefore, network interconnectedness was further examined. TNL provided insight into the total vessel density supported by each SC type. Further examination into the number of connected vessel sets per volume elucidated the level of network interconnectedness each SC type facilitated. Fewer connected sets per volume indicated that the network was more interconnected rather than separate, dispersed vessel segments. LFs and DFs did not elicit significant differences in network interconnectedness over the second week in culture (Fig. 3a, c, respectively); however, MSC-supported microvascular networks did show significant differences in the degree of network interconnectedness for two of the four conditions (Fig. 3b). Vessel networks formed with support from MSCs with higher initial cell densities (conditions 1 and 2) exhibited a decrease in the number of connected sets over the second week in culture (day 7 vs. day 14). However, LFs supported the formation of significantly more interconnected networks overall (~20 connected sets/mm^3 compared to ~50-100 connected sets/mm^3 for DF- and MSC-supported networks) (Fig. 3d, e).

Though LFs consistently aided in the formation of interconnected networks, DF- and MSC-supported networks did trend towards a decrease in connected sets over time (Fig. 3d, e).

On day 7, LF-supported networks had significantly fewer connected sets than both DF- and MSC-supported networks in all four conditions (Fig. 3d). However, by day 14, differences were only observed in 1:1 SC:EC ratios (Fig. 3e). These data indicate a trend towards decreasing connected sets in DF- and MSC-supported networks despite the lack of significance when compared with conditions of the same cell type across time periods.

Stromal cell type determines network perfusability

In addition to morphological assessments of the microvascular networks, we also assessed critical functional aspects such as vessel perfusion. We hypothesized that a more interconnected network would facilitate better perfusion of the region between the two parent channels. To perfuse the microvascular network, three criteria were needed: 1) patent parent channels, 2) inosculation of microvessels to the parent channels, and 3) patent microvessels. Here we showed that stromal cell identity influenced these criteria, which were assessed via the infusion of 10 kDa fluorescent dextran into the parent channels.[30–32] LF-containing devices had patent parent channels in 100% of samples (Fig. 4b, Fig. S2a) and perfused microvascular networks in greater than 50% of samples on day 7 and day 14 (Fig. 4a, c, Fig. S2b). Conversely, MSC- and DF-containing devices yielded microvascular networks that did not perfuse (Fig. 4c, Fig. S2b), despite some percentage of parent channel patency (Fig. 4b, Fig. S2a). Samples with two patent parent channels were considered completely open. DF-containing samples had at least one patent parent channel 56% of the time (27% completely open) on day 7, but this percentage dropped considerably by day 14 to only 6% with a single patent channel (0% completely open). MSC-containing samples had 100% patency in at least one parent channel on day 7 (83% completely open) which decreased slightly by day 14 to 88% with at least one patent channel (69% completely open).

In this system, the second and third criteria could only be assessed in tandem, i.e., dextran only flowed through the network if microvessels were both patent and inosculated to the

parent channel. It is possible that in DF- and MSC-supported networks, there were patent microvessels that were not inosculated, inosculated microvessels that were not patent, or microvessels that were neither patent nor inosculated. However, in this system, these separate scenarios could not be distinguished.

Total cell number impacted the ability of stromal cells to aid in network formation

To further characterize differences in microvascular networks formed in the presence of each SC type, we examined total cell number and change in cell number at the final time point of culture. In samples formed with each of the three SC types, changes in cell number over the culture duration led to an equilibration of cell density within the devices by the final day in culture (either day 7 or day 14) (Fig. 5a). MSC-supported networks exhibited the lowest final cell density. In LF-containing and DF-containing samples, the final cell density for each condition was roughly equal to the mean (or slightly below) of the four cell densities used at the start of the experiment, while for MSC-containing samples the final cell density for each condition was around the lowest initial cell density (or slightly below) used at the start of the experiment. LF- and DF- supported networks exhibited both increases and decreases in cell number over time, indicating an optimal total initial cell density between 1.5-2M total cells/mL that would result in no change in cell number. In these constructs, total initial cell densities less than 2M cells/mL led to an increase in cell number, while total initial cell densities above 2M cells/mL led to a decrease in cell number (Fig. 5b, left and right). Conversely, MSC-supported networks exhibited decreases in cell number across all conditions (Fig. 5b, middle).

Stromal cell traction forces may influence microvascular network formation

Previous studies from our group and others have implicated EC-mediated contractile forces in angiogenic sprouting and the formation of microvascular networks in natural matrices.[10,33,34] However, the impact of stromal cell contractile forces on vascular

morphogenesis is comparatively understudied, despite relevance for vascular development, engineered tissues, and tumor angiogenesis. Therefore, we aimed to determine if SC-generated traction forces may account for the observed differences in network formation, channel patency, and network perfusion in various SC-supported networks. Differences in LF-, DF-, and MSC-generated traction forces were quantified by culturing cells on collagen-functionalized polyacrylamide gels containing 0.2 μm beads as fiduciary markers and performing 2D traction force microscopy (TFM). LFs and DFs produced significantly greater levels of median traction compared to MSCs (Fig. 5c, d).

Stromal cells express αSMA and reside in perivascular locations in this on-chip platform

Prior studies have shown SCs from a range of tissue origins are capable of adopting a perivascular morphology and expressing a subset of pericyte markers, when co-cultured in hydrogels.[34–36] Therefore, we sought to qualitatively assess αSMA expression and stromal cell localization in relation to the vessel networks that formed within the microfluidic devices, focusing on a subset of samples fabricated using the cell density and ratio of condition 2. All three SC types displayed αSMA protein expression at day 7 in culture (Fig. 6a). LFs, DFs, and MSCs displayed a spread and elongated morphology within the gels, with the DFs appearing to spread most extensively and uniformly throughout the gels in the representative images shown. By day 14, LF expression of αSMA appeared qualitatively diminished with less perivascular association (Fig. 6b). In contrast, DFs and MSCs remained closely associated with the microvasculature (Fig. 6b), adopting a sheath-like morphology marked by αSMA expression around vessels (Fig. 6b, white arrowheads). In the case of cultures containing MSCs, αSMA expression appeared to be restricted to cells in perivascular locations, especially at day 14; in contrast, cultures containing DFs showed αSMA expression in cells found throughout the gel.

DISCUSSION

Stromal cells play a critical role in tissue vascularization in development and wound healing, and a clear understanding of their roles in capillary formation is critical to developing more complex engineered tissues with tissue-specific, specialized functions and a more complete vascular hierarchy. While vessel formation in EC-SC co-cultures within microfluidic chips has been previously studied,[37–39] direct comparisons between SC types across distinct studies are difficult to make due to differences in microfluidic geometries, EC sources, SC sources, medium formulations, fluid flow, culture duration, and the type of anastomosis. In this study, we used an on-chip platform for static co-culture of ECs and SCs using a consistent medium source, EC source, and microfluidic geometry in order to make head-to-head comparisons in the abilities of three different SC types to direct vascular assembly. Parent channels approximating arteriole diameters were fully encapsulated within a fibrin matrix within this device, thereby supporting physiologically relevant anastomoses between de novo formed microvascular network structures within the matrix and these parent channels. Consistent with other reports investigating co-culture models of vascular morphogenesis in natural matrices in on-chip systems,[16–18] ECs formed microvascular networks within this on-chip platform using either LFs, DFs, or MSCs as the supportive cells. LFs and DFs supported more expansive network formation compared to MSC-supported samples. Over time in culture, MSCs supported changes to microvascular network organization, including a greater degree of network interconnectedness, while fibroblast-supported networks remained more constant over a longer duration for the parameters measured.

In an effort to better understand how SCs of different tissue origins give rise to endothelial networks that are quantitatively and qualitatively distinct, we investigated two candidate possibilities by focusing on cell densities and traction forces. Our analysis of cell density identified differences between samples containing fibroblasts and MSCs. Co-cultures containing fibroblasts showed an increase in cell number when the initial seeding density was

low, but a reduction in cell number when the initial seeding density was high. Co-cultures containing MSCs decreased in cell number regardless of the initial seeding density. These changes in cell density correlate with the degree of vascularization as quantified by measuring total network lengths (note the similar shapes to the graphs in Figure 2B vs. Figure 5B), and therefore may partially explain the significantly lower TNL in MSC-supported samples compared to fibroblast-supported samples, as well as inconsistencies in vascular morphogenesis and function. More broadly, these observations suggest two possibilities: SC density is tightly regulated to support vascular morphogenesis, lumenogenesis, and patency, or SCs regulate EC density to control the same parameters. However, our data do not address if the EC or SC are preferentially dying or proliferating in our microfluidic devices.

One study of neovascularization in modular fibrin microtissues containing EC-fibroblast co-cultures of 1:1 and 1:3 ratios, similar to the ratios used here, showed preferential proliferation of the fibroblasts.[25] Another study showed that fibroblasts regulate vascular morphogenesis and lumenogensis in part by secreting paracrine angiogenic factors to enable sprouting and ECM proteins that stiffen the matrix to enable lumenogensis.[40] In our results, elevated paracrine secretions of pro-angiogenic factors and ECM could potentially be due to elevated numbers of SCs in our LF-EC and DF-EC co-cultures relative to the MSC-EC co-cultures. On the other hand, a particularly innovative recent study used an inducible caspase-9 kill-switch gene to preferentially induce apoptosis in fibroblasts, and revealed that transient support of fibroblasts (as little as 3 days) is sufficient to drive the formation of functional microvasculature.[41] That study used cell densities that were 3-9x higher than those we used here, and thus it seems likely the time required for the presence of the fibroblasts depends on the number present. However, a potentially important complicating factor in dissecting the mechanisms by which SCs modulate vascular morphogenesis in co-culture systems is the choice of culture medium. We used EGM-2 for consistency across conditions, but the different SCs may alter their

16

secretome and/or their ability to synthesize and remodel the ECM in this medium relative to their basal culture medium.

Differences in SC-generated traction forces may also play a role in the observed differences in vascular morphogenesis and perfusion. It has been well-established that EC-generated traction forces play important roles in vascular morphogenesis,[42–45] in part by reorganizing ECM fibers to enhance EC migration and invasion.[46] However, the roles of SC-generated forces in vascular assembly are comparatively understudied. Quantification of traction stresses using 2D traction force microscopy suggested a correlation between SC-generated forces and TNL, as both LFs and DFs generate larger traction stress and support vascular assembly to a greater extent than MSCs. Since fibroblasts support more extensive endothelial network formation than do MSCs, higher levels of tension in the ECM imparted by higher levels of traction force exerted by SCs may play a role. However, LFs and DFs produced similar levels of traction, despite yielding microvascular networks with clear differences in channel patency and network perfusion. This suggests that the magnitude of SC-mediated traction forces cannot fully explain the observed differences in microvascular function in our system. DFs, LFs, and MSCs reside in different tissue microenvironments and serve different functions *in vivo,* and our use of 2D TFM as a surrogate for traction forces in 3D multicellular microenvironments at a single time point may not capture nuanced differences between SC types in terms of the timing and duration of traction forces. The use of 3D TFM approaches[47] and/or microrheology[10] in future work may shed some additional light on differences in SC forces during vascular morphogenesis, but are beyond the scope of this particular study.

The qualitative differences in αSMA expression observed in our study may also implicate differences in SC-generated traction forces. αSMA expression has been linked to increased traction forces and a myofibroblast phenotype in fibroblasts.[48,49] One study showed increased expression of αSMA enhanced the contractile activity of cultured fibroblasts.[50] Qualitatively, DFs

showed the greatest degree of αSMA expression on both days 7 and 14, and a more uniform distribution of αSMA+ cells throughout the entire gel compared to both LFs and MSCs. DF-generated traction forces distributed over a larger gel volume, while perhaps initially beneficial to accelerate vascular assembly by stiffening the fibrous ECM and enhancing long-range communication, may accelerate fibrin compaction and/or remodeling when sustained over prolonged periods in a manner akin to fibrosis that adversely affect parent channel patency. In contrast, αSMA expression in LFs appeared to decrease over time, coinciding with sustained parent channel patency. The αSMA expression levels and localization patterns we observed are also consistent with the observed differences in microvessel diameter. Capillary pericytes have been shown to control blood flow by modulating capillary diameter.[51] In our co-cultures, MSCs and DFs exhibited a greater degree of perivascular association and sustained this association for a longer duration compared to LFs, perhaps leading to the smaller vessel diameters observed in MSC-EC and DF-EC co-cultures compared to LF-EC co-cultures.

Perfusion of endothelial microvessels is critical for long-term tissue function *in vitro* and *in vivo*. In this study, samples were cultured statically for 7 or 14 days followed by a brief addition of flow to assess dextran infusion into parent channels and microvascular networks. Here we show that LFs were the only SC type tested that could facilitate perfusion of endothelial microvessels in the absence of flow preconditioning. However, our previous *in vivo work*[7] has shown successful lumenization and perfusion of EC-MSC vessels, suggesting that the absence of continuous flow in our system may explain the lack of perfusion in MSC- and DF-supported vessels. A recent study which showed perfusion of DF-supported vessels used a much higher cell density and incorporated flow into the system,[41] while a study that showed perfusion of MSC-supported vessels also examined vessels under static culture but used a microfluidic device where anastomosis occurred to openings in a PDMS channel[16] rather than physiologic anastomosis to an endothelialized, matrix-encapsulated channel. Our results, coupled with the

results from others cited above, further highlight the need for consistency in study parameters to specifically parse out the role of SCs in vascular morphogenesis and vessel perfusion. In future studies, we will investigate how EC morphogenesis and vessel perfusion are impacted by flow in this system and the influence of multiple SC types within a single device.

To summarize, we report the use of a microfluidic chip platform to evaluate if differences in SC identity induce changes in vascular morphogenesis and function in 3D natural hydrogel matrices. We used this system to characterize vasculature formed by co-culturing ECs with tissue-specific SCs.[52] We demonstrated that co-cultures of ECs and fibroblasts generated more expansive vascular networks compared to co-cultures of ECs and MSCs. We further showed that vascular morphogenesis induced by LFs and DFs yielded capillary networks that may correlate with the distinct functions of their organ-specific origins. LF-supported microvasculature displayed wider diameters, which may be important to facilitate gas exchange in the alveoli;[53] by contrast, DF-supported microvasculature coincided with closure of the arteriole-scale parent channels, potentially due to DF-mediated contraction of the fibrin matrix consistent with the role of DFs in remodeling provisional clots during wound healing and DFs undergoing a transition to a myofibroblast phenotype.[54] Future studies could also incorporate tissue-specific ECs,[52] such as normal human lung microvascular ECs co-cultured with LFs rather than the more widely used HUVECs. Overall, the reproducibility, simplicity, and flexibility (cell type, matrix composition, matrix density, etc.) of this microfluidic microvascular system provides a platform to probe fundamental vascular biology questions during neovascularization, to gain an understanding of tissue-specific vasculature, and to guide strategies to vascularize engineered tissues and organs.

CONFLICTS OF INTEREST

There are no conflicts to declare.

CRediT AUTHOR CONTRIBUTIONS

Emily A. Margolis: Conceptualization, Formal Analysis, Investigation, Methodology, Software, Validation, Visualization, Writing – Original Draft, Writing – Review and Editing. David S. Cleveland: Methodology. Yen P. Kong: Formal Analysis, Investigation, Methodology, Software, Validation. Jeffrey A. Beamish: Methodology. William Y. Wang: Methodology. Brendon M. Baker: Methodology, Resources. Andrew J. Putnam: Conceptualization, Funding Acquisition, Methodology, Project Administration, Resources, Visualization, Writing – Review and Editing.

FIGURE CAPTIONS AND TABLE WITH CAPTION

Figure 1: Methods for the formation and analysis of microvascular networks. (A) Schematic diagram and (B) corresponding phase-contrast images of gelation, seeding, and culture procedures (steps 2-4). (C) Color image of the PDMS mold bonded to a glass slide with acupuncture needles inserted. (D) Maximum intensity projection of a confocal z-stack and binarization for network analysis for LF-EC networks (left) and MSC-EC networks (right).

Table 1: Cellular ratio and density conditions used to fabricate samples throughout the study.

CONDITION	SC-EC RATIO	SC DENSITY	EC DENSITY
1	2:1	2 M/mL	1 M/mL
2	1:1	1 M/mL	1 M/mL
3	2:1	1 M/mL	500 K/mL
4	1:1	500 K/mL	500 K/mL

Figure 2: Microvascular morphogenesis is impacted by stromal cell identity. (A) Representative UEA stained images of microvascular networks formed from LF-EC (left), MSC-EC (middle), and DF-EC (right) co-cultures on day 7 (top) and day 14 (bottom). (B) Quantification of total network length on day 7 (left) and day 14 (right). (C) Data in (B) repopulated into separate graphs to make comparisons within a single cell type. (D) Quantification of vessel diameter on day 14. (E) Representative UEA (red) and DAPI (blue) stained images of microvascular networks formed from LF-EC (left), MSC-EC (middle), and DF-EC (right) condition 4 co-cultures on D14 depicting differences in vessel diameter. $\alpha < 0.05$ was considered significant. * $p < 0.05$, ** $p < 0.01$, *** $p < 0.001$, **** $p < 0.0001$, \$ $p < 0.05$, & $p < 0.01$. Matched symbols and brackets with symbols indicate significance. Two (TNL) or three (diameter) ROIs were assessed per technical replicate, with a minimum of 3 technical replicates per condition, per time point, per cell type and N = 3 independent replicates per condition, per time point, per cell type analyzed. Data points correspond to independent replicates.

Figure 3: Bone marrow-derived mesenchymal stem cells induce changes in network interconnectedness over time. Quantification of network interconnectedness over time for (A) LF-EC, (B) MSC-EC, and (C) DF-EC co-cultures. (D, E) Data repopulated from (A)-(C) to make comparisons of network interconnectedness between each stromal cell type on (D) day 7 and (E) day 14. $\alpha < 0.05$ was considered significant. * $p < 0.05$, ** $p < 0.01$, *** $p < 0.001$, **** $p < 0.0001$. Two ROIs per technical replicate, a minimum of 3 technical replicates per condition, per time point, per cell type and N = 3 independent replicates per condition, per time point, per cell type were analyzed. Data points correspond to independent replicates.

Figure 4: Stromal cell type determines vessel patency and microvascular network perfusion. (A) LF-EC networks perfused with 10 kDa dextran on day 14 in condition 3 (left) and condition 4 (right). Images show complete perfusion. (B) Channel patency and (C) network perfusion for each cell type on day 7 (top) and day 14 (bottom). (B, C) Data from all four conditions pooled by cell type. A minimum of 3 technical replicates per condition, per time point, per cell type and N = 3 independent replicates included per condition, per time point, per cell type were analyzed.

Figure 5: Network morphogenesis is influenced by cell number and cell-imparted traction. (A) Total cell number at the endpoint of culture for all three stromal cell types. (B) Change in cell number for all three network formations. (C) Cell imparted traction on collagen-coated polyacrylamide matrices. (D) Representative images of cell traction for each SC type. $\alpha < 0.05$ was considered significant. * $p < 0.05$, ** $p < 0.01$. N = 28-30 cells per cell type analyzed; data points represent individual cells.

Figure 6: DFs and MSCs exhibit closer perivascular association than do LFs in SC-EC co-cultures. Alpha smooth muscle actin (αSMA) expression on (A) day 7 and (B) day 14.

Representative immunofluorescence staining for αSMA (green) counterstained with UEA (red)

and DAPI (blue) to show the position of SCs relative to vessels. All samples are from condition

2. White arrowheads depict the sheath-like association of αSMA+ SCs to UEA+ microvessels.

REFERENCES
1.   FA Auger, L Gibot, and D Lacroix. The Pivotal Role of Vascularization in Tissue Engineering. *Annu Rev Biomed Eng*. 2013,**15**:177–200.
2.   J Rouwkema, NC Rivron, and CA Van Blitterswijk. Vascularization in tissue engineering. *Trends Biotechnol*. 2008,**26**(8):434–41.
3.   RK Jain, P Au, J Tam, DG Duda, and D Fukumura. Engineering vascularized tissue. Vol. 23, Nature Biotechnology. 2005. p. 821–3.
4.   KLS Chan, AH Khankhel, RL Thompson, BJ Coisman, KHK Wong, JG Truslow, et al. Crosslinking of collagen scaffolds promotes blood and lymphatic vascular stability. *J Biomed Mater Res - Part A*. 2014,**102**(9):3186–95.
5.   RM Linville, NF Boland, G Covarrubias, GM Price, and J Tien. Physical and Chemical Signals That Promote Vascularization of Capillary-Scale Channels. *Cell Mol Bioeng*. 2016,**9**(1):73–84.
6.   DHT Nguyen, SC Stapleton, MT Yang, SS Cha, CK Choi, PA Galie, et al. Biomimetic model to reconstitute angiogenic sprouting morphogenesis in vitro. *Proc Natl Acad Sci U S A*. 2013,**110**(17):6712–7.
7.   SJ Grainger, B Carrion, J Ceccarelli, and AJ Putnam. Stromal cell identity influences the in vivo functionality of engineered capillary networks formed by co-delivery of endothelial cells and stromal cells. *Tissue Eng Part A*. 2013,**19**(9–10):1209–22.
8.   S Alimperti, T Mirabella, V Bajaj, W Polacheck, DM Pirone, J Duffield, et al. Three-dimensional biomimetic vascular model reveals a RhoA, Rac1, and N-cadherin balance in mural cell–endothelial cell-regulated barrier function. *Proc Natl Acad Sci U S A*. 2017,**114**(33):8758–63.
9.   JR Bezenah, YP Kong, and AJ Putnam. Evaluating the potential of endothelial cells derived from human induced pluripotent stem cells to form microvascular networks in 3D cultures. *Sci Rep*. 2018,**8**(1):2671.
10.   BA Juliar, MT Keating, YP Kong, EL Botvinick, and AJ Putnam. Sprouting angiogenesis induces significant mechanical heterogeneities and ECM stiffening across length scales in fibrin hydrogels. *Biomaterials*. 2018,**162**:99–108.
11.   SJ Grainger, and AJ Putnam. Assessing the permeability of engineered capillary networks in a 3D culture. *PLoS One*. 2011,**6**(7):e22086.
12.   JA Beamish, BA Juliar, DS Cleveland, ME Busch, L Nimmagadda, and AJ Putnam. Deciphering the relative roles of matrix metalloproteinase- and plasmin-mediated matrix degradation during capillary morphogenesis using engineered hydrogels. *J Biomed Mater Res - Part B Appl Biomater*. 2019,**107**(8):2507–16.
13.   BA Juliar, JA Beamish, ME Busch, DS Cleveland, L Nimmagadda, and AJ Putnam. Cell-mediated matrix stiffening accompanies capillary morphogenesis in ultra-soft amorphous hydrogels. *Biomaterials*. 2020,**230**:119634.
14.   M Vigen, J Ceccarelli, and AJ Putnam. Protease-Sensitive PEG Hydrogels Regulate Vascularization In Vitro and In Vivo. *Macromol Biosci*. 2014,**14**(10):1368–79.
15.   AY Rioja, R Tiruvannamalai Annamalai, S Paris, AJ Putnam, and JP Stegemann. Endothelial sprouting and network formation in collagen- and fibrin-based modular microbeads. *Acta Biomater*. 2016,**29**:33–41.
16.   JS Jeon, S Bersini, JA Whisler, MB Chen, G Dubini, JL Charest, et al. Generation of 3D functional microvascular networks with human mesenchymal stem cells in microfluidic systems. *Integr Biol (United Kingdom)*. 2014,**6**(5):555–63.
17.   X Wang, DTT Phan, A Sobrino, SC George, CCW Hughes, and AP Lee. Engineering anastomosis between living capillary networks and endothelial cell-lined microfluidic channels. *Lab Chip*. 2016,**16**(2):282–90.
18.   S Kim, H Lee, M Chung, and NL Jeon. Engineering of functional, perfusable 3D microvascular networks on a chip. *Lab Chip*. 2013,**13**(8):1489–500.

19.   CM Ghajar, KS Blevins, CCW Hughes, SC George, and AJ Putnam. Mesenchymal stem cells enhance angiogenesis in mechanically viable prevascularized tissues via early matrix metalloproteinase upregulation. *Tissue Eng*. 2006,**12**(10):2875–88.

20.   QH Chen, AR Liu, HB Qiu, and Y Yang. Interaction between mesenchymal stem cells and endothelial cells restores endothelial permeability via paracrine hepatocyte growth factor in vitro. *Stem Cell Res Ther*. 2015,**6**(1):44.

21.   S Maacha, H Sidahmed, S Jacob, G Gentilcore, R Calzone, J-C Grivel, et al. Paracrine Mechanisms of Mesenchymal Stromal Cells in Angiogenesis. 2020,.

22.   RR Rao, AW Peterson, J Ceccarelli, AJ Putnam, and JP Stegemann. Matrix composition regulates three-dimensional network formation by endothelial cells and mesenchymal stem cells in collagen/fibrin materials. *Angiogenesis*. 2012,**15**(2):253–64.

23.   M Loibl, A Binder, M Herrmann, F Duttenhoefer, RG Richards, M Nerlich, et al. Direct Cell-Cell Contact between Mesenchymal Stem Cells and Endothelial Progenitor Cells Induces a Pericyte-Like Phenotype In Vitro. *Biomed Res Int*. 2014,.

24.   WY Wang, D Lin, EH Jarman, WJ Polacheck, and BM Baker. Functional angiogenesis requires microenvironmental cues balancing endothelial cell migration and proliferation. *Lab Chip*. 2020,.

25.   R Tiruvannamalai Annamalai, AY Rioja, AJ Putnam, and JP Stegemann. Vascular Network Formation by Human Microvascular Endothelial Cells in Modular Fibrin Microtissues. *ACS Biomater Sci Eng*. 2016,**2**(11):1914–25.

26.   Y Aratyn-Schaus, PW Oakes, J Stricker, SP Winter, and ML Gardel. Preparation of complaint matrices for quantifying cellular contraction. *J Vis Exp*. 2010,(46).

27.   Q Tseng, E Duchemin-Pelletier, A Deshiere, M Balland, H Guilloud, O Filhol, et al. Spatial organization of the extracellular matrix regulates cell-cell junction positioning. *Proc Natl Acad Sci U S A*. 2012,**109**(5):1506–11.

28.   YP Kong, AY Rioja, X Xue, Y Sun, J Fu, and AJ Putnam. A systems mechanobiology model to predict cardiac reprogramming outcomes on different biomaterials. *Biomaterials*. 2018,**181**:280–92.

29.   MA Traore, and SC George. Tissue Engineering the Vascular Tree. Vol. 23, Tissue Engineering - Part B: Reviews. Mary Ann Liebert Inc.; 2017. p. 505–14.

30.   SC Pearce, A Al-Jawadi, K Kishida, S Yu, M Hu, LF Fritzky, et al. Marked differences in tight junction composition and macromolecular permeability among different intestinal cell types.

31.   TD Brown, ‡ | Maksymilian Nowak, A V Bayles, | Balabhaskar Prabhakarpandian, P Karande, ME Helgeson, et al. A microfluidic model of human brain (μHuB) for assessment of blood brain barrier. *Bioeng Transl Med*. 2019,**4**.

32.   GM Price, KHK Wong, JG Truslow, AD Leung, C Acharya, and J Tien. Effect of mechanical factors on the function of engineered human blood microvessels in microfluidic collagen gels. *Biomaterials*. 2010,**31**(24):6182–9.

33.   GE Davis, and CW Camarillo. Regulation of endothelial cell morphogenesis by integrins, mechanical forces, and matrix guidance pathways. *Exp Cell Res*. 1995,**216**(1):113–23.

34.   CM Ghajar, S Kachgal, E Kniazeva, H Mori, S V. Costes, SC George, et al. Mesenchymal cells stimulate capillary morphogenesis via distinct proteolytic mechanisms. *Exp Cell Res*. 2010,**316**(5):813–25.

35.   N Kosyakova, DD Kao, M Figetakis, F López-Giráldez, S Spindler, M Graham, et al. Differential functional roles of fibroblasts and pericytes in the formation of tissue-engineered microvascular networks in vitro. *npj Regen Med*. 2020,**5**(1):1–12.

36.   L Moroni, H Fernandes, J Rouwkema, W Holnthoner, K Pill, J Melke, et al. Microvascular Networks From Endothelial Cells and Mesenchymal Stromal Cells From Adipose Tissue and Bone Marrow: A Comparison. *Front Bioeng Biotechnol | www.frontiersin.org*. 2018,**6**:156.

37.   S Lee, J Ko, D Park, S-R Lee, M Chung, cd Younggyun Lee, et al. Lab on a Chip
       CRITICAL REVIEW Microfluidic-based vascularized microphysiological systems.
       2018,**18**:2686.
38.   K Haase, and RD Kamm. Advances in on-chip vascularization. *Regen Med*.
       2017,(3):285–302.
39.   S Bersini, and M Moretti. 3D functional and perfusable microvascular networks for
       organotypic microfluidic models. *J Mater Sci Mater Med*.
40.   AC Newman, MN Nakatsu, W Chou, PD Gershon, CCW Hughes, and J Stein. The
       requirement for fibroblasts in angiogenesis: fibroblast-derived matrix proteins are
       essential for endothelial cell lumen formation. 2011,**22**.
41.   HG Song, A Lammers, S Sundaram, L Rubio, AX Chen, L Li, et al. Transient Support
       from Fibroblasts is Sufficient to Drive Functional Vascularization in Engineered Tissues.
       Adv Funct Mater. 2020,:2003777.
42.   C Yoon, C Choi, S Stapleton, T Mirabella, C Howes, L Dong, et al. Myosin IIA–mediated
       forces regulate multicellular integrity during vascular sprouting. *Mol Biol Cell*.
       2019,**30**(16):1974–84.
43.   AL Sieminski, RP Hebbel, and KJ Gooch. The relative magnitudes of endothelial force
       generation and matrix stiffness modulate capillary morphogenesis in vitro. *Exp Cell Res*.
       2004,**297**(2):574–84.
44.   E Kniazeva, and AJ Putnam. Endothelial cell traction and ECM density influence both
       capillary morphogenesis and maintenance in 3-D. *Am J Physiol - Cell Physiol*.
       2009,**297**(1).
45.   MM Vaeyens, A Jorge-Peñas, J Barrasa-Fano, C Steuwe, T Heck, P Carmeliet, et al.
       Matrix deformations around angiogenic sprouts correlate to sprout dynamics and suggest
       pulling activity. *Angiogenesis*. 2020,**23**(3):315–24.
46.   CD Davidson, WY Wang, I Zaimi, DKP Jayco, and BM Baker. Cell force-mediated matrix
       reorganization underlies multicellular network assembly. *Sci Rep*. 2019,**9**(1).
47.   WR Legant, JS Miller, BL Blakely, DM Cohen, GM Genin, and CS Chen. Measurement of
       mechanical tractions exerted by cells in three-dimensional matrices. *Nat Methods*.
       2010,**7**(12):969–71.
48.   J Wang, R Zohar, and CA McCulloch. Multiple roles of α-smooth muscle actin in
       mechanotransduction. Vol. 312, Experimental Cell Research. Academic Press Inc.; 2006.
       p. 205–14.
49.   CD Davidson, DKP Jayco, DL Matera, SJ DePalma, HL Hiraki, WY Wang, et al.
       Myofibroblast activation in synthetic fibrous matrices composed of dextran vinyl sulfone.
       Acta Biomater. 2020,**105**:78–86.
50.   B Hinz, G Celetta, JJ Tomasek, G Gabbiani, and C Chaponnier. Alpha-smooth muscle
       actin expression upregulates fibroblast contractile activity. *Mol Biol Cell*.
       2001,**12**(9):2730–41.
51.   J Almaça, J Weitz, R Rodriguez-Diaz, E Pereira, and A Caicedo. The Pericyte of the
       Pancreatic Islet Regulates Capillary Diameter and Local Blood Flow. *Cell Metab*.
       2018,**27**(3):630-644.e4.
52.   DSY Lin, F Guo, and B Zhang. Modeling organ-specific vasculature with organ-on-a-chip
       devices. 2018,.
53.   A Fantin, A Manco, A Frizzelli, and E Crisafulli. Supply of the alveoli with blood and
       circulation in the alveoli | Ivanov | Journal of Respiratory Research [Internet]. [cited 2020
       Sep 8]. Available from: http://www.ghrnet.org/index.php/jrr/article/view/2154/2534
54.   LE Tracy, RA Minasian, and EJ Caterson. Extracellular Matrix and Dermal Fibroblast
       Function in the Healing Wound. Vol. 5, Advances in Wound Care. Mary Ann Liebert Inc.;
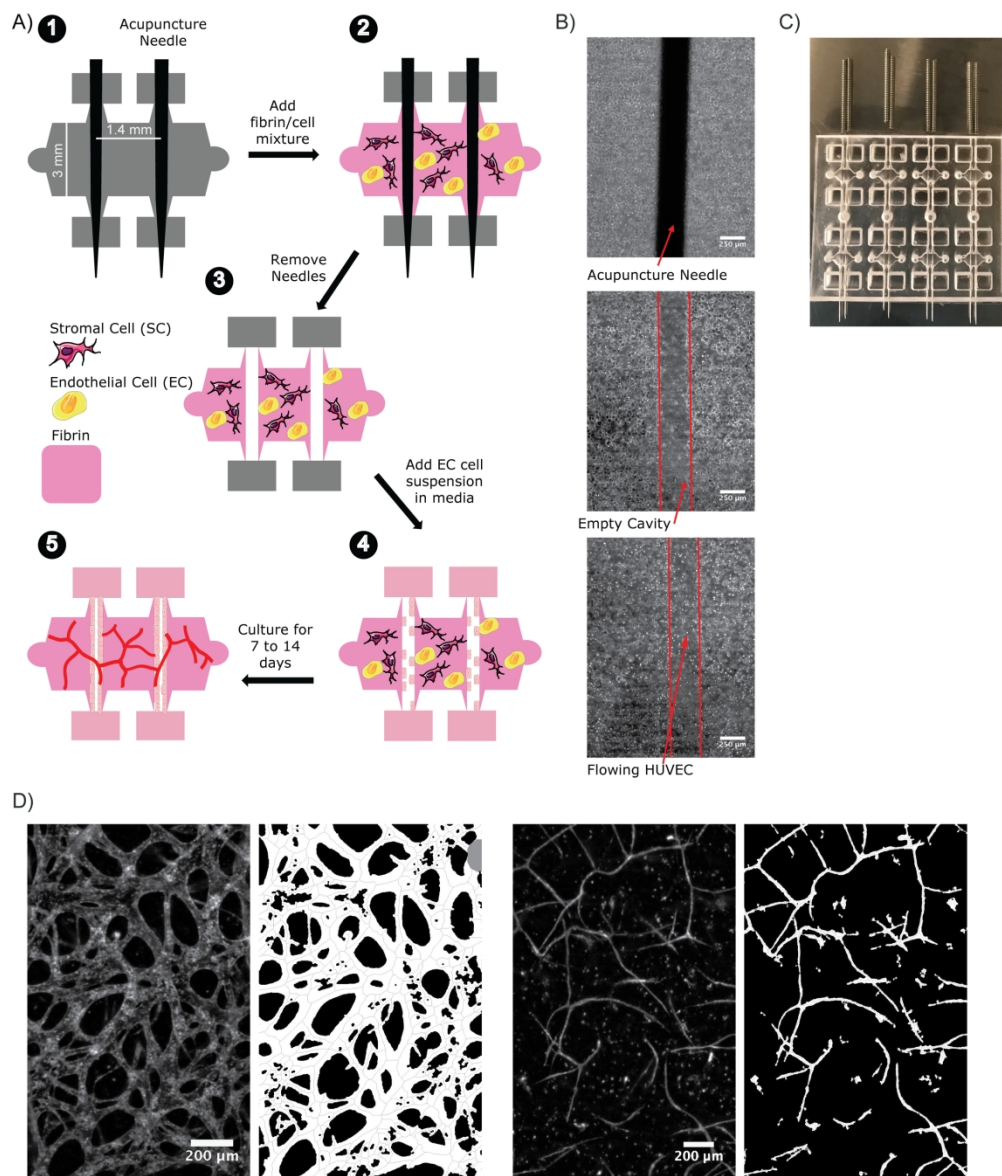   2016. p. 119–36.

Figure 1: Methods for the formation and analysis of microvascular networks. (A) Schematic diagram and (B) corresponding phase-contrast images of gelation, seeding, and culture procedures (steps 2-4). (C) Color image of the PDMS mold bonded to a glass slide with acupuncture needles inserted. (D) Maximum intensity projection of a confocal z-stack and binarization for network analysis for LF-EC networks (left) and MSC-EC networks (right).
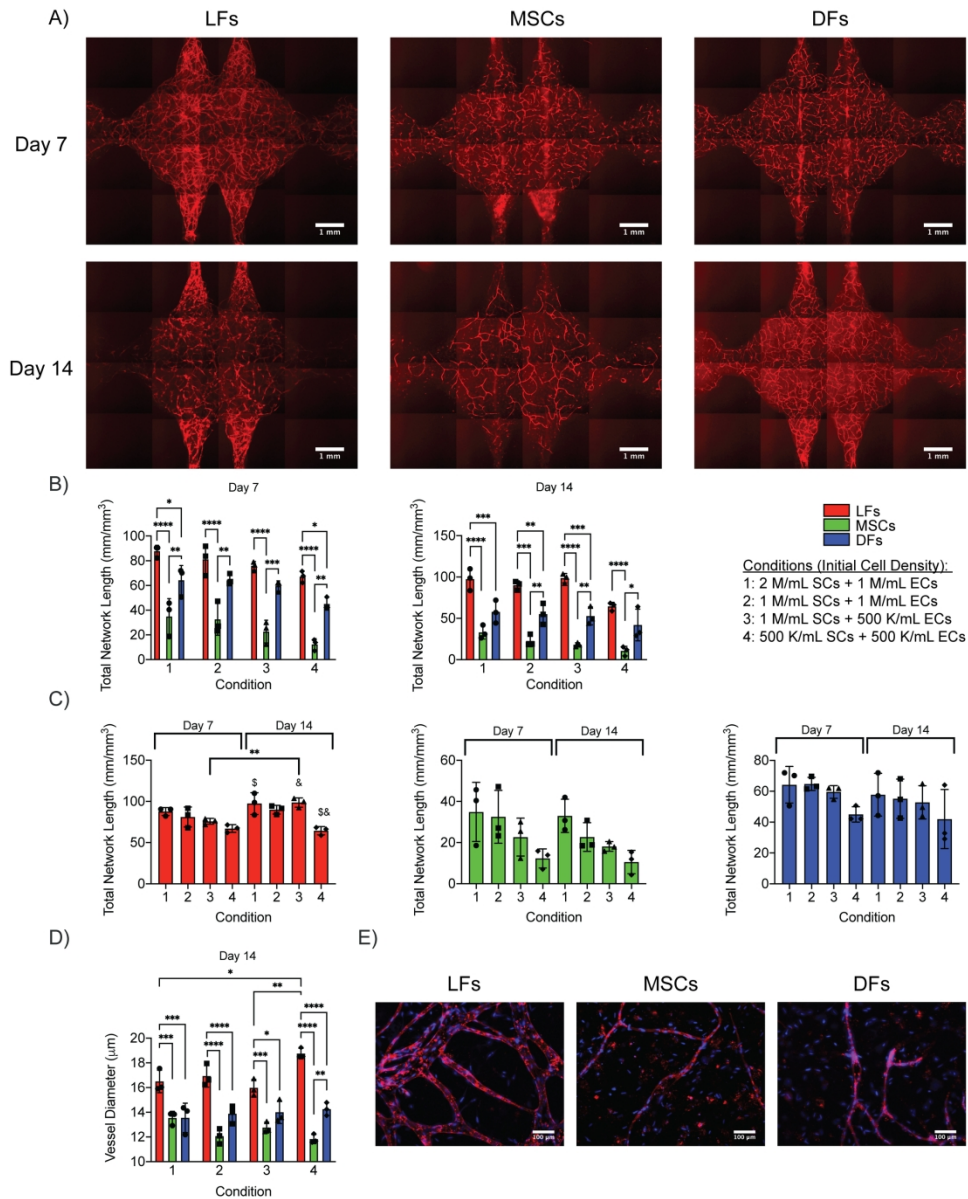
204x238mm (300 x 300 DPI)

Figure 2: Microvascular morphogenesis is impacted by stromal cell identity. (A) Representative UEA stained images of microvascular networks formed from LF-EC (left), MSC-EC (middle), and DF-EC (right) co-cultures on day 7 (top) and day 14 (bottom). (B) Quantification of total network length on day 7 (left) and day 14 (right). (C) Data in (B) repopulated into separate graphs to make comparisons within a single cell type. (D) Quantification of vessel diameter on day 14. (E) Representative UEA (red) and DAPI (blue) stained images of microvascular networks formed from LF-EC (left), MSC-EC (middle), and DF-EC (right) condition 4 co-cultures on D14 depicting differences in vessel diameter. $\alpha < 0.05$ was considered significant. * $p < 0.05$, ** $p < 0.01$, *** $p < 0.001$, **** $p < 0.0001$, $ $p < 0.05$, & $p < 0.01$. Matched symbols and brackets with symbols indicate significance. Two (TNL) or three (diameter) ROIs were assessed per technical replicate, with a minimum of 3 technical replicates per condition, per time point, per cell type and N = 3 independent replicates per condition, per time point, per cell type analyzed. Data points correspond to independent replicates.
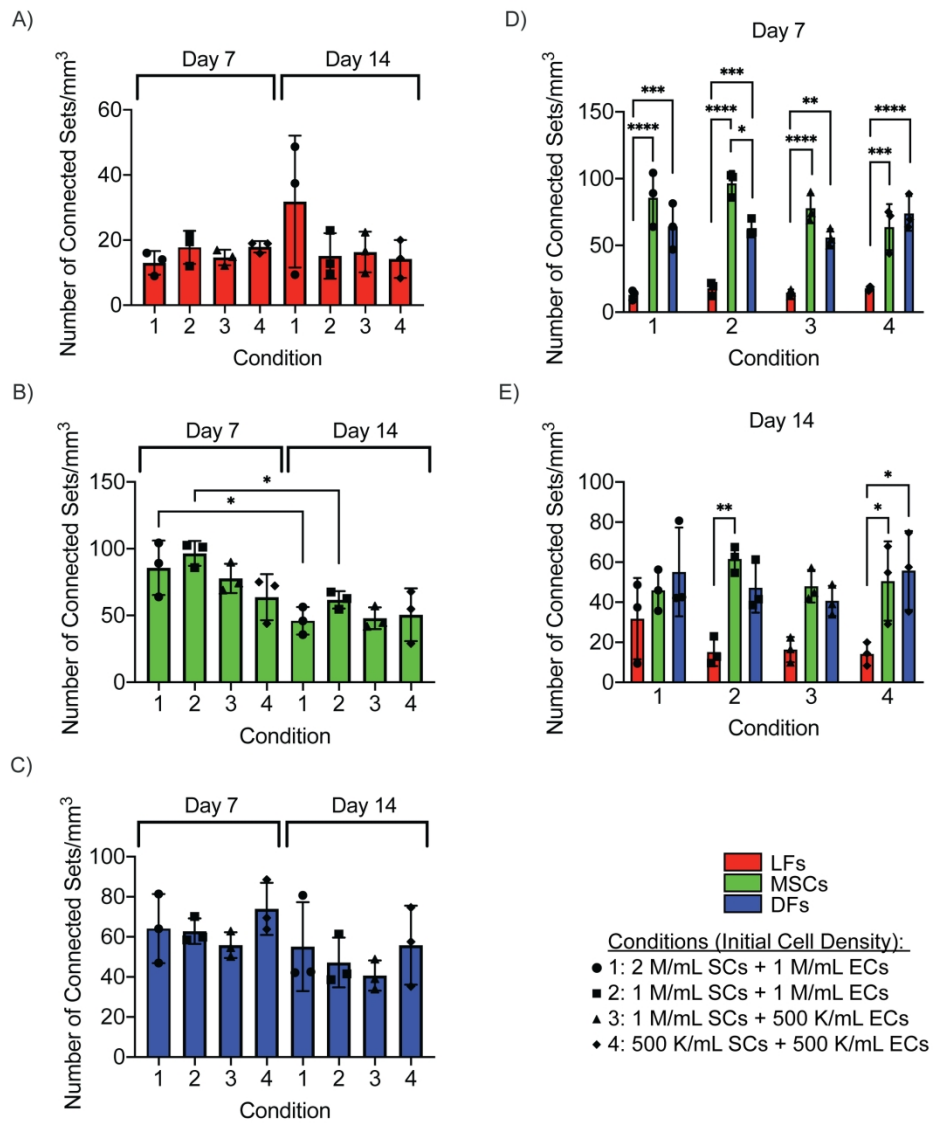
206x250mm (300 x 300 DPI)

Figure 3: Bone marrow-derived mesenchymal stem cells induce changes in network interconnectedness over time. Quantification of network interconnectedness over time for (A) LF-EC, (B) MSC-EC, and (C) DF-EC co-cultures. (D, E) Data repopulated from (A)-(C) to make comparisons of network interconnectedness between each stromal cell type on (D) day 7 and (E) day 14. $\alpha < 0.05$ was considered significant. * $p < 0.05$, ** $p < 0.01$, *** $p < 0.001$, **** $p < 0.0001$. Two ROIs per technical replicate, a minimum of 3 technical replicates per condition, per time point, per cell type and N = 3 independent replicates per condition, per time point, per cell type were analyzed. Data points correspond to independent replicates.
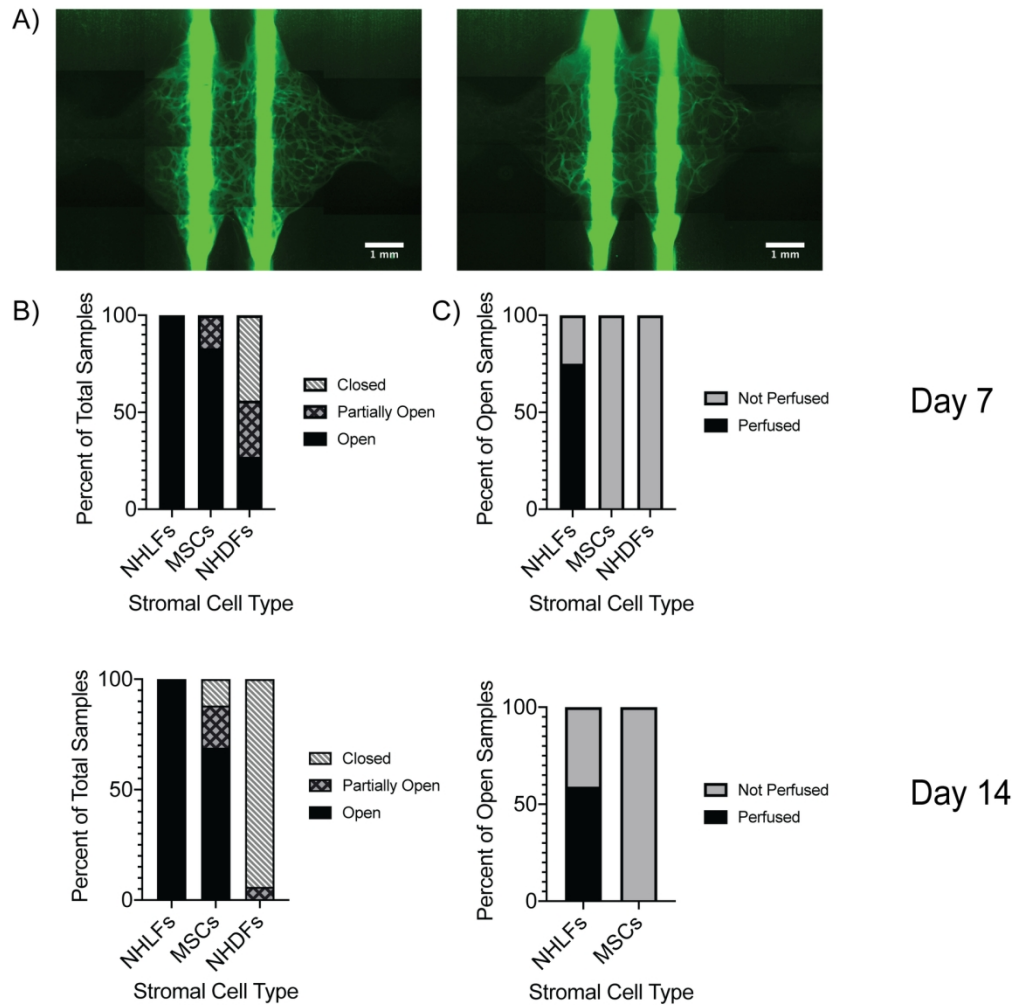
194x238mm (300 x 300 DPI)

Figure 4: Stromal cell type determines vessel patency and microvascular network perfusion. (A) LF-EC networks perfused with 10 kDa dextran on day 14 in condition 3 (left) and condition 4 (right). Images show complete perfusion. (B) Channel patency and (C) network perfusion for each cell type on day 7 (top) and day 14 (bottom). (B, C) Data from all four conditions pooled by cell type. A minimum of 3 technical replicates per condition, per time point, per cell type and N = 3 independent replicates included per condition, per time point, per cell type were analyzed.
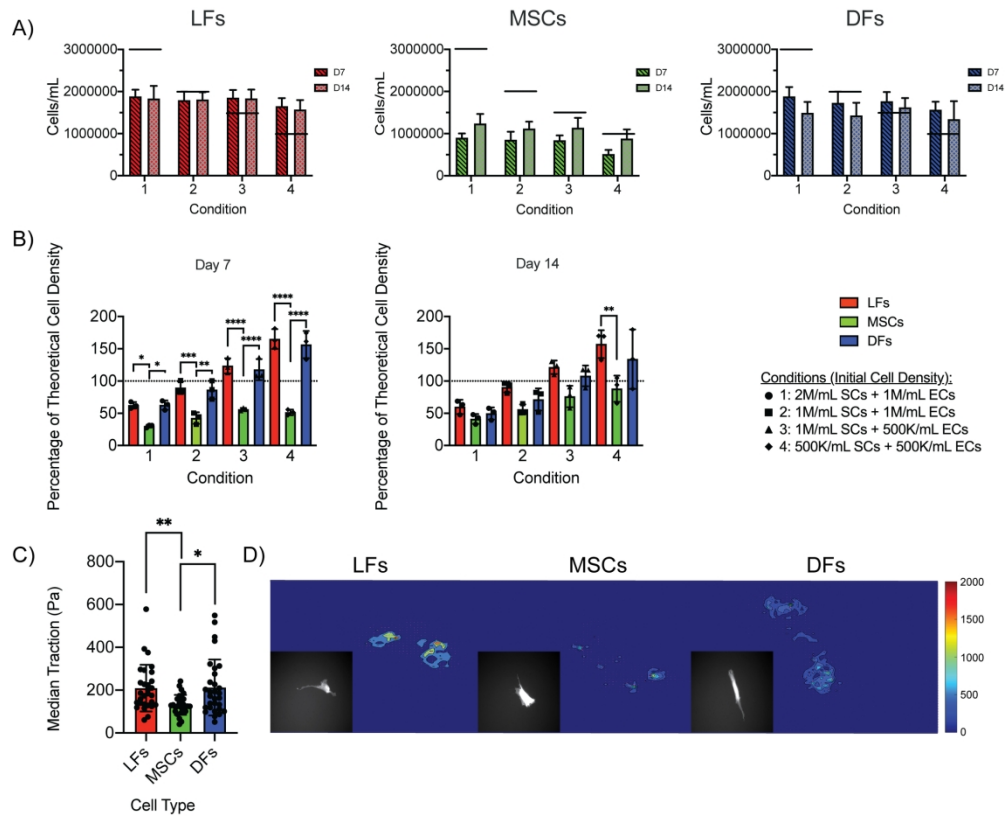
154x156mm (300 x 300 DPI)

Figure 5: Network morphogenesis is influenced by cell number and cell-imparted traction. (A) Total cell number at the endpoint of culture for all three stromal cell types. (B) Change in cell number for all three network formations. (C) Cell imparted traction on collagen-coated polyacrylamide matrices. (D) Representative images of cell traction for each SC type. $α < 0.05$ was considered significant. * $p < 0.05$, ** $p < 0.01$. N = 28-30 cells per cell type analyzed; data points represent individual cells.
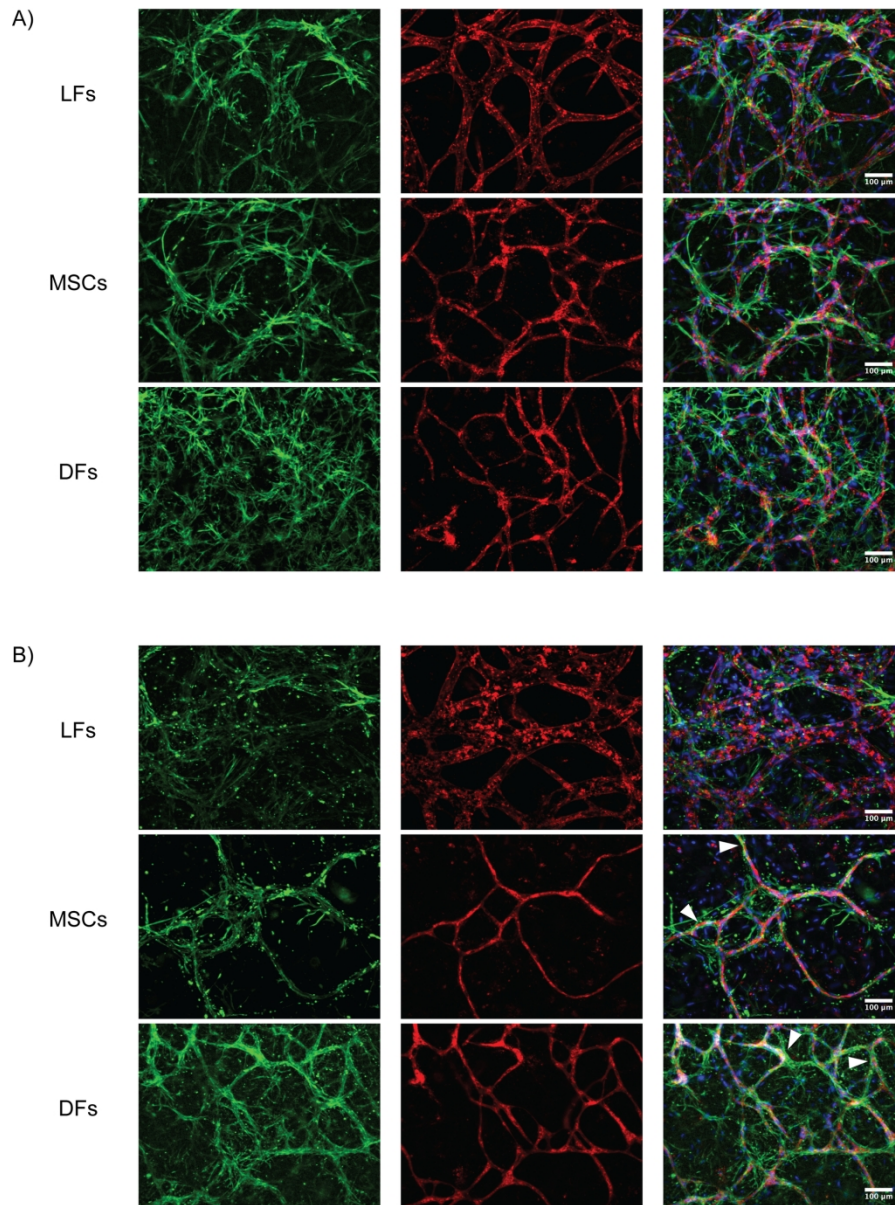
196x159mm (300 x 300 DPI)

Figure 6: DFs and MSCs exhibit closer perivascular association than do LFs in SC-EC co-cultures. Alpha smooth muscle actin (αSMA) expression on (A) day 7 and (B) day 14. Representative immunofluorescence staining for αSMA (green) counterstained with UEA (red) and DAPI (blue) to show the position of SCs relative to vessels. All samples are from condition 2. White arrowheads depict the sheath-like association of αSMA+ SCs to UEA+ microvessels.

182x235mm (300 x 300 DPI)